ISSN : 0974 - 7486 Volume 13 Issue 2

Materials Science

An Indian Journal

Full Paper

MSAIJ, 13(2), 2015 [049-063]

Al_2O_3 nano-particle reinforced aluminium matrix composites through stir casting technique

A.K.Barnwal, D.P.Mondal*, Hemant Jain, S.Das, A.K.Jha, R.Dasgupta, P.Banerjee

CSIR- Advanced Materials and Processes Research Institute, Hoshangabad Road, 462026, (BHOPAL)

E-mail : dpmondal@ampri.res.in; mondaldp@yahoo.com

ABSTRACT

2014 aluminium alloy metal matrix composites (AMMCs) reinforced with Al_2O_3 nano-particles (ANP) were fabricated using stir casting technique. The volume fraction of ANP varied between 0.5 and 1.5 vol%. The compressive deformation behaviour of these composites was investigated as a function of ANP content at different temperatures and strain rates. Scanning Electron Microscope observations revealed uniform dispersion of ANP in the matrix. Strong bonding between ANP and the matrix was also observed. The yield strength, and ultimate compressive strength increased with increase in ANP content, and decreased with increase in test temperature. The compressive deformation behaviour was marginally influenced by strain rate. Work softening behaviour of the composite was observed at high temperature, which was caused due to dynamic recrystallization and strain aging.

KEYWORDS

Metal matrix composites;
Nano-particle reinforced;
Casting;
Microstructure;
Yield stress and
Ultimate stress.

INTRODUCTION

Aluminium alloy matrix composites have emerged as potential materials for applications in aerospace, automobile, defence, military industry due to their excellent properties. Low density, lower thermal expansion, high specific strength, high specific stiffness, high thermal conductivity, wear resistance[1-5] are the attractive properties of such composites. There are various kinds of reinforcement particles such as Al_2O_3, SiC, MgO, B_4C. Aluminium alloy matrix composites have higher specific strength and stiffness at the cost of ductility[3-6] as compared to the unreinforced alloy. The use of aluminium matrix composite as structural application is limited due to its low ductility. There are several methods of fabrication of metal matrix composites such as liquid metallurgy[7], Powder metallurgy[8], and vortex process and ultrasonic stirring[9]. Out of these methods, vortex technique (stir-casting) is the most cost competitive and commercially viable process. But the major drawback of this process is to get uniformly dispersed fine particles especially nano-sized particles in the matrix.

Attempts have been made to improve the uniformity in distribution of such fine particles through special design and adaptation of ultrasonic or electromagnetic stirring[1]. Formability of AMCs improves significantly when reinforced with uniformly distributed fine particles[10]. Coarser particles impart defects which make them susceptible to crack during deformation leading to reduced strength and toughness. Coarse particles also

results in lower degree of coherency with matrix. It finally results in less strengthening effect in the matrix[11]. Higher compressive strength of alloy as compared to the coarse SiC particle (50 to 90 μm) reinforced composite after age hardening has also been reported by Mondal et.al.[12]. According to these investigators, effective precipitation of the base alloy during age hardening and shear of coarse particles at lower stress level than the age hardened matrix, makes coarse particles of the base alloy to be superior to that of the composites[12]. The strength and toughness of AMCs are strongly influenced by the particle distribution and its volume fraction[13]. The strength, modulus and wear resistance of AMCs increases with increase in reinforcement volume fraction[13]. Provided the particles are uniformly distributed in the matrix and have at least 25% coherency[8] with the matrix. The clustered region act as voids or cracks, and thus the strength as well as ductility of the alloy reduce significantly. In order to get the higher strength and toughness, the AMCs should have the following characteristics: (i) uniform distribution of particles, (ii) finer particle sizes, (iii) coherency between particle and matrix, and (iv) better extent of dislocation strengthening.

The extent of matrix strengthening or dislocation strengthening increases with the improvement in coherency of the particle with the matrix and reduction in defects in particles and matrix[13]. Use of ultrafine or submicron particles / fibre inherently leads to clustering in the matrix of the composites[9]. Several attempts have been made to get uniform distribution of particle reinforcement in the matrix[14,15]. A few of the methods include roll bonding process[13,16] in situ technique[13-17]. SHS process[18], electromagnetic stirring and ultrasonic stirring[1]. However, some extent of clustering are always occurred there even though these techniques are adopted very precisely and precautionally. As a result, expected improvement in strength, modulus and formability are not realised in AMC's even when these AMCs are reinforced with nano-particles[12]. In addition, these process demand accurate process control and sophisticated instrumentation. In addition, bulk manufacturing is restricted in the above processes. Above point led to develop a stir casting technique to make nano-particle reinforced AMCs with uniform particle distribution and improve mechanical properties. Improvement of wetability between particles and matrix and uniform distribution of the particles in the liquid melt were also aimed at. Incorporation of pallets of Al_2O_3 nano particle with Al powder in aluminium alloy melt and simultaneous mechanical stirring was thought to get bulk nano particle reinforced composite with better uniform distribution. This paper deals with synthesis of Al_2O_3 nano particle reinforced AA2014 alloy matrix composite using modified stir casting technique. These composites were characterised for microstructure and compressive deformation as a function of strain rate, temperature and ANP volume fraction.

EXPERIMENTAL

Materials synthesis and microstructural characterisation

2014 Al alloy -Al_2O_3 nano- particle reinforced composite (AANPRC) was prepared using modified stir casting technique. The Flow sheet of the technique used for making AANPRC is shown in Figure 1. Aluminium alloy (AA) was first melted at ~ 700 °C in an electrical resistance furnace and then the melt was mixed with ANP (0.5 vol% to 1.5 vol. %) through the mechanical stirrer rotating at an angular velocity of 400 to 450 rpm. Alloy melt and composite liquid of AA with ANP were poured into the preheated cylindrical die. As ANPs are difficult to disperse in liquid aluminium alloy melt through mechanical stirring, a minor modification in this technique was done. In this approach, instead of preheated nano- particle powder, pallets of (10 mm diameter and 5 mm height) ANP and aluminium powder mixture were added in the liquid metal. While melt was stirred, these pallets were dipped inside the metal bath through the use of perforated cylindrical steel holder. The aluminium in the pallets got easily dissolved in the AA melt and the ANP was released slowly from the pallets and were distributed uniformly in the melt due to stirring action. After completion of ANP addition, the AA melt is continued to stir for another few minutes (~five minutes) to ensure uniform distribution of ANP in AANPRC. Through this technique, AANPRC of 5 kg batch was made. The AA and AANPRCs were cast in cylindrical cast iron die of 20 mm diameter and 200 mm height. Samples of 20 mm diameter and 10 mm height are cut

from the middle of the cast AA and AANPRCs for micro-structural examination. The cut samples are polished and etched using standard metallographic technique[19]. The etched samples are gold sputtered prior to scanning electron microscopic (SEM) examination. The deformed samples were cut transversely, mounted, and polished and etched using standard methodology[19]. The deformed samples after etching were also examined using SEM in order to understand deformation mechanism during compressions at different strain rates and temperatures.

Compression test

Cylindrical samples (of 10 mm diameter and 15 mm height) were made from cast AA and AANPRCs for compression tests. The tests were conducted at different strain rates (0.01/s, 0.1/s & 1/s) and at different temperatures (100, 200 & 300 ^{0}C) using an Instron Universal Testing Machine (Model No.8801). During high temperature tests, the test samples were allowed to heat at a particular temperature for 15 minutes in order to ensure uniform heating of these test samples during deformation. In order to reduce the friction between sample surface and test platen, the specimen surface as well as the platen surface were coated with solid lubricant MoS_2. The deformed samples were cut transversely, polished and etched using the same methodology used for micro-structural observations. Nano-hardness measurements were carried out on the polished samples prior to and after deformation using a load of 50 mN in a CETR-Nanoindenter (Model:Nanosurf-Nanite B). Nano-hardness measurement was made at the and away from the interface in order to find out the interface strength and coherency as well as to understand the matrix work-hardening or softening mechanism. The hardness and modulus of the matrix were also determined through nano-hardness measurement.

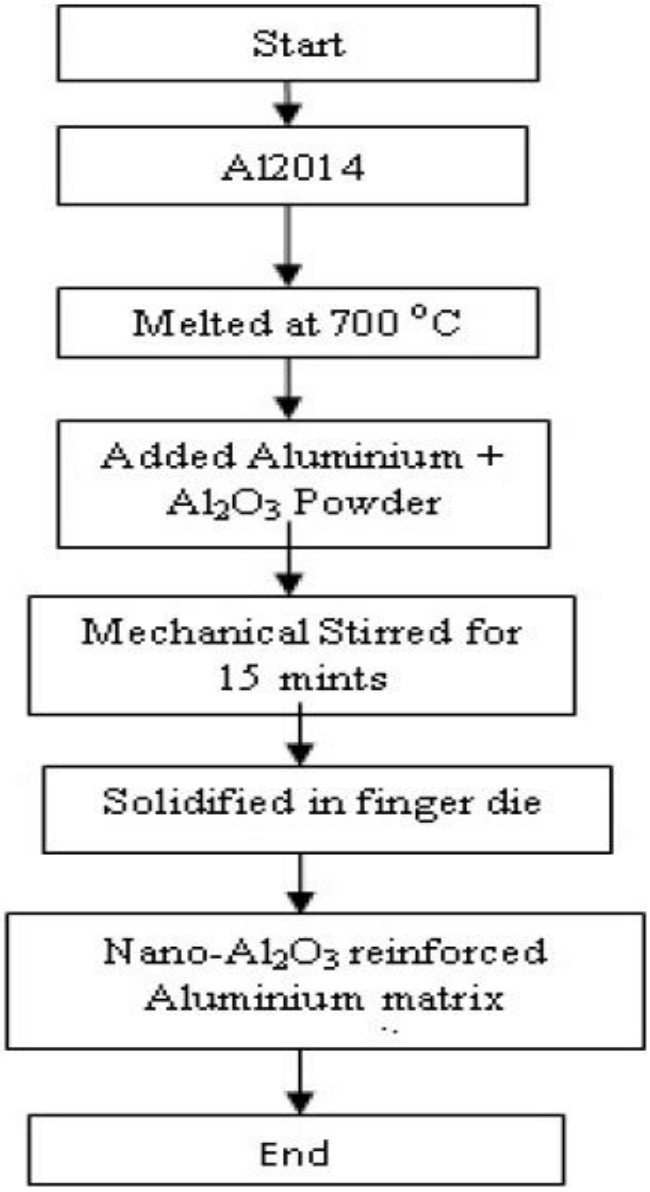

Figure 1 : Flow sheet for making AANPRC

RESULTS AND DISCUSSION

Materials and microstructure

The microstructure of ascast AA shows dendrites of primary α-Al and eutectic phase of α- Al and $CuAl_2$ in the interdendritic region (Figure 2a). The average secondary dendrite arm spacing was noted to be 45± 4 μm. The eutectic of $CuAl_2$ and α-Al show lamellar structure (Figure 2b). Almost similar kind of microstructure was observed in AANPRC with 0.5 vol% ANP (Figure 2c). However, in the case of AANPRC, the secondary arms spacing of α-Al dendrite was refined marginally (35±4 μm). It is interesting to note that ANPs are uniformly distributed in the matrix, especially in α-Al dendrite (Figure 2d) unlike that in the case of coarse particle reinforced composite where the particles were pushed towards the interdendritic regions. It is further noted that the average size of ANP in AANPRC is ~40± 4 nm (Figure 2d). The average sizes of asreceived

Full Paper

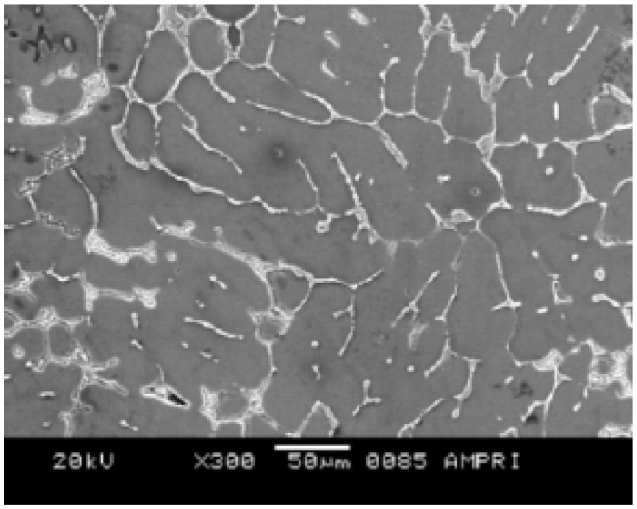

(a)

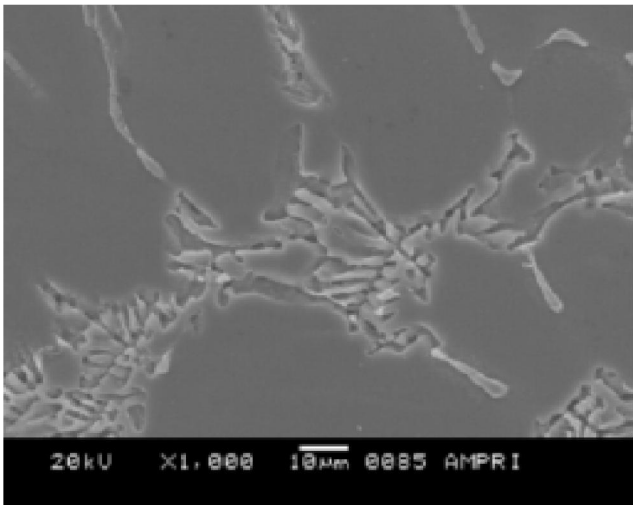

(b)

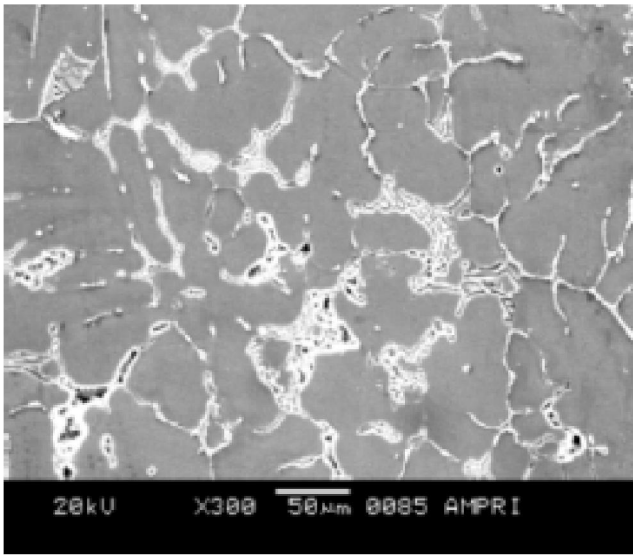

(c)

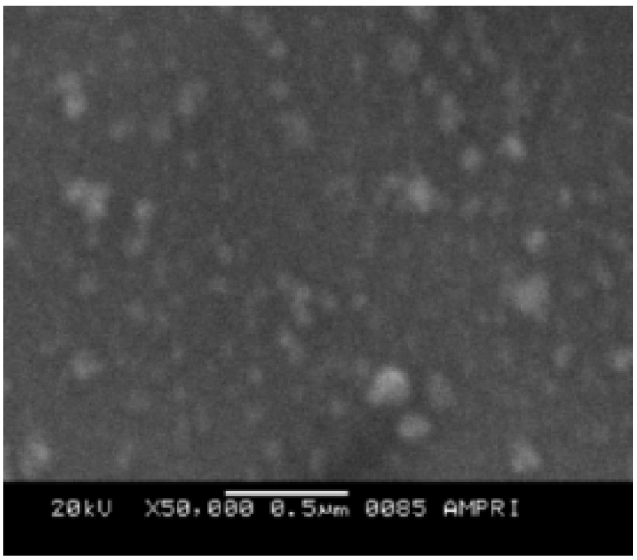

(d)

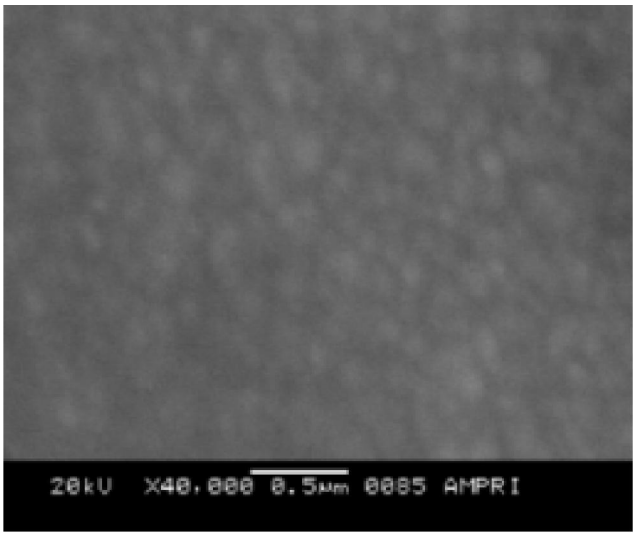

(e)

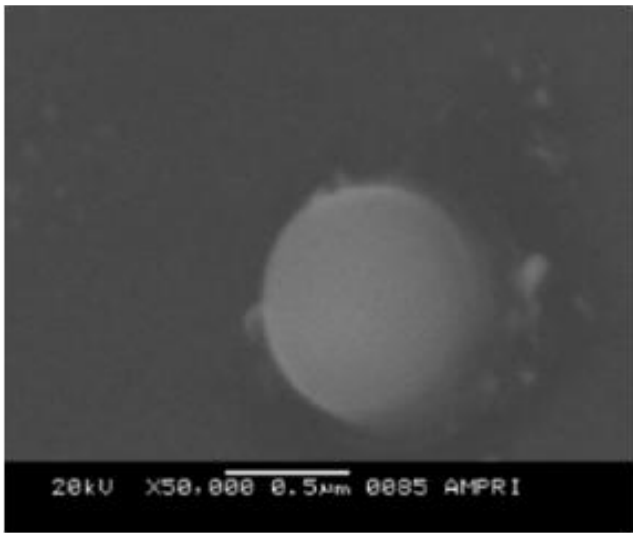

(f)

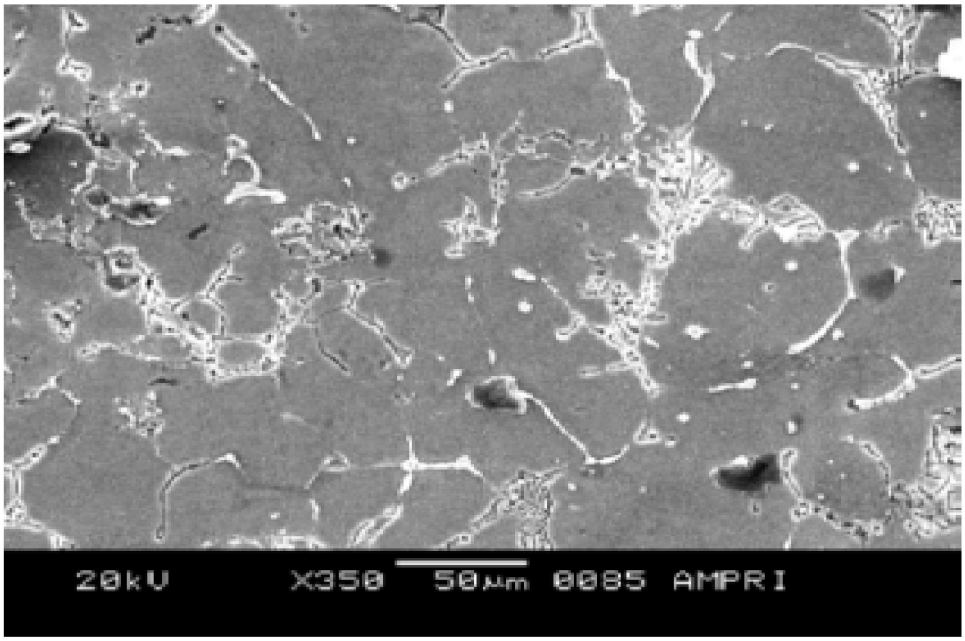

Figure 2 : Microstructure of AANPRC (a) as cast alloy, (b) eutectic phase of α- Al and CuAl2, (c) AANPRC with 0.5 vol% ANP, (d) uniformly distributed ANP in α-Al, (e) AANPRC with 1.0 vol% ANP, (f) coarser ANP in α- Al dendrite, (g) AANPRC with 1.5 vol% ANP having some degree of particle agglomeration.

TABLE 1 : Effect of ANP % on the micro-hardness of the AANPRC

S.N	% ANP	Micro-hardness (HV)	% improvement of Hardness
1	0	110	0
2	0.5	125	13.51
3	0.75	135	23.2
4	1.5	140	27.3

ANPs were 34± 5 nm. The average size of ANPs in AANPRC is marginally higher than that of as-received one. This may be due to presence of clustering of ANP in the matrix. But the clustering is nominal as the average size of as received ANP and that of ANP in AANPRC is very close to each other. The microstructure of the matrix (-dendrite) of AANPRC with 1.0 vol. % ANP also depicts uniform distribution of ANP (Figure 2e). A few ANP are also found to be coarser in size (~240 nm) as shown in Figure 2f. However, it exhibits a very sharp coherent interface with the matrix. While ANP content increased to 1.5 vol %, relatively greater extent of particle agglomeration (marked arrows) is noted (Figure 2g). In addition, the secondary dendrite arm spacing is noted to be coarser than that observed in the composites with 0.5 and 1.0 vol % Al_2O_3. The secondary arm spacing in AANPRC was noted to be almost similar to that of as cast AA. This may be due to clustering of particle.

The micro-hardness of the matrix AA and AANPRC was measured in order to get a comparison of matrix strengthening due to addition of ANP. The micro-hardness of matrix and the dendritic arm spacing as a function of ANP are shown in TABLE 1. It is noted that the strength of dendrite arm increases with increases in ANP content. However, improvement in micro-hardness due to change of ANP content from 0.5 to 1.5 vol % is marginal (only 10%). This is primarily attributed to increased agglomeration of ANP in AANPRC with increased ANP content and coarser secondary arm spacing.

Stress-strain diagram

The true stress- true strain curves of AANPRC with 0.5 vol % ANP when drawn at different temperatures (100, 200 & 300 °C) and at a fixed strain rate (i.e. 0.01/s) are shown in Figure 3a. It is evident, that there

Full Paper

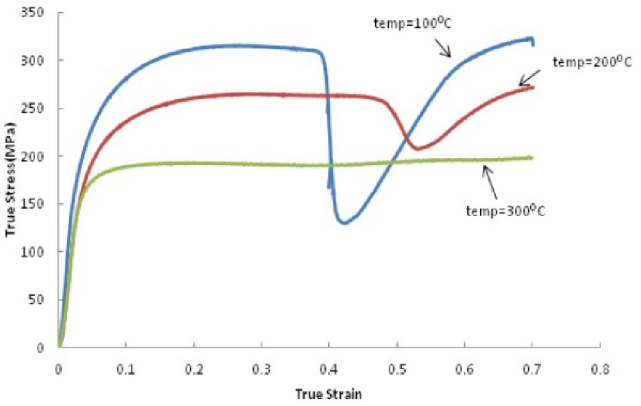

Figure 3a : True stress-strain diagram curves of AANPRC with 0.5 wt% ANP at different temperature and at a fixed strain rate of 0.01/s

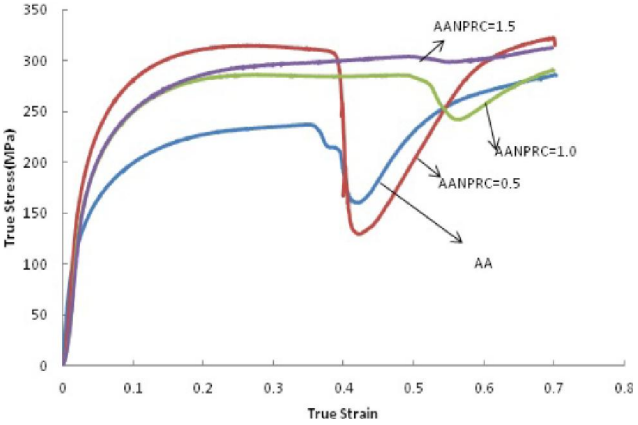

Figure 3b : Stress –strain curves of AANPRCs at 100°C and at a fixed strain rate of 0.01/s

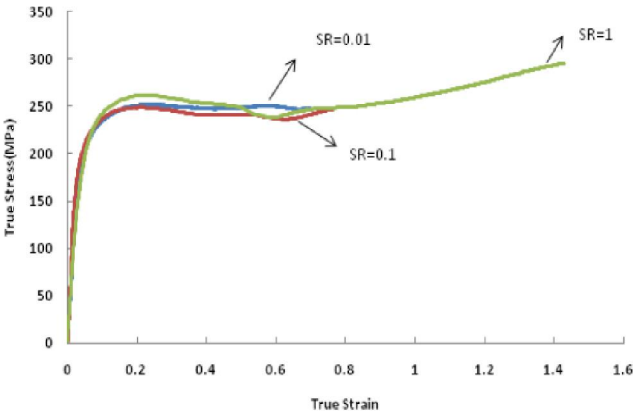

Figure 3c : Stress-strain curves of AANPRC with 1 wt% ANP at a temperature of 200°C and at different strain rates

is no distinct yield point on these curves. Rather, there exists a continuous transition from yield to plastic region as was observed in most of the cases in AA. It is clearly noted from the Figure 3a that the flow stress of AANPRC decreases with increase in temperature. The stress-strain curves of AANPRCs when drawn at a temperature of 100 °C and at a strain rate of 0.01/s are shown in Figure 3b. Stress-Strain curve of as-cast AA, for comparison with the AANPRC, are shown on the same plot. It is noted that the flow stress of AANPRCs increases with increase in ANP content. Similar trend was also noted at other strain rates and temperatures. It was further noted that at 100°C there was a sharp valley in the stress-strain curve which was due to shearing of sample and generation of cracks in the shear plane during compression testing. After shearing, the sample again gets compacted and the stress increases. The stress-strain curves of AANPRC with 1.0 vol % ANP at a temperature of 200°C for different strain rates are shown in Figure 3c. It is evident from this figure that the flow curves vary marginally with strain rates indicating that the deformation response was marginally influenced with the strain rate. It is interesting to note that there is no sharp valley in stress-strain curves when tested at 200°C. However, there is a tendency of either softening or work hardening after yielding (i.e. in the plastic region). The yield stress (0.2% proof stress), maximum compressive stress and elongation are recorded from these stress- strain curves and reported in TABLE 2. It is evident from this table that the yield stress and maximum compressive stress increase significantly with increase in ANP content, whereas these value increase. The magnitude of these parameters (yield stress and compressive stress) decreases with increase in test temperature. The plastic strain increases with increase in temperature and decreases with increase in ANP content. At higher temperature, fracture of AA and AANPRC could not be observed, that is why the elongation of the investigated materials are not reported in TABLE 2.

Strain hardening exponent

In order to calculate the strain hardening exponent (n) the stress-strain curves were converted to *ln (stress)* to *ln (strain)* curves, and then two best fitted lines (one for bottom half and other for top half) were produced. The slope of the top line gives the value of 'n' and the antilog of the intercept of the top line gives the plastic strengthening coefficient (K_p). For each curve, these values were noted in order to see the effect of temperature, strain rates and ANP content on each of these

TABLE 2 : Effect of strain rate, temperature and ANP content on the yield stress and compressive stress

S.N.	Al_2O_3 (vol %)	Strain rate	Temp (°C)	Yield Stress (MPa)	UCS (MPa)
1.	0.0	0.01	100	160	240
2.			200	140	200
3.			300	110	145
4.		0.1	100	190	265
5.			200	150	190
6.			300	120	155
7.		1.0	100	200	280
8.			200	160	220
9.			300	123	160
10.	0.5	0.01	100	170	290
11.			200	150	225
12.			300	130	165
13.		0.1	100	200	300
14.			200	160	235
15.			300	130	170
16.		1.0	100	230	298
17.			200	190	255
18.			300	140	168
19.	1.0	0.01	100	200	300
20.			200	168	245
21.			300	145	185
22.		0.1	100	220	325
23.			200	176	250
24.			300	147	190
25.		1.0	100	235	315
26.			200	180	260
27.			300	152	185
28.	1.5	0.01	100	220	302
29.			200	180	253
30.			300	185	201
31.		0.1	100	230	315
32.			200	190	258
33.			300	150	205
34.		1.0	100	240	325
35.			200	210	265
36.			300	160	210

parameters (TABLE 3). TABLE 3 depicts that *n* decreases with increase in temperature irrespective of strain rate and ANP content. At temperature of 300^{0}C, the value of '*n*' is negligible and sometimes it showed a negative value indicating strain softening. In few cases, even at 200^{0}C '*n*' is negative and a very low value of '*n*' is noted. K_P also decreases with increase in temperature, and increases with increase in strain rate and ANP content.

Effect of Al_2O_3 content

The variation of yield stress as a function of ANP content at different temperatures and at fixed strain rate of 0.01/s is shown in Figure 4a. It is noted that the yield

Full Paper

TABLE 3 : Effect of temperature, strain rate and % ANP content on strain hardening exponent 'n' and Plastic Strengthening coefficient

S.N.	Al_2O_3 (vol %)	Strain rate (S^{-1})	Temp.(^oC)	n	K_P (MPa)
		0.01		0.199	311.687
		0.1	100	0.207	341.0
		1		0.195	354.958
		0.01		0.133	248.0
1.	0	0.1	200	0.125	266.66
		1		1.95	282.0
		0.01		-0.016	127.749
		0.1	300	-0.024	130.843
		1		0.018	150.505
		0.01		0.198	352.482
		0.1	100	0.227	382.221
		1		0.229	382.884
		0.01		0.156	249.358
2.	0.5	0.1	200	0.148	269.616
		1		0.149	285.430
		0.01		0.016	143.308
		0.1	300	0.046	157.590
		1		0.031	174.687
		0.01		0.170	371.667
		0.1	100	0.227	392.986
		1		0.229	431.384
		0.01		0.106	278.105
3.	1.0	0.1	200	0.072	284.667
		1		-0.020	299.166
		0.01		0	172.389
		0.1	300	0.020	192.096
		1		0.003	192.096
		0.01		0.203	392.986
		0.1	100	0.205	428.804
		1		0.210	431.384
		0.01		0.14	303.384
4.	1.5	0.1	200	0.12	317.665
		1		0.133	323.435
		0.01		-0.028	192.289
		0.1	300	-0.028	195.195
		1		0.005	205.819

stress increases steadily but slowly with increase in ANP content. Similar trend of variation in yield stress at other strain rates are also noted. Figure 4b represents the variation of yield stress with ANP content at a fixed test temperature of 200 ^oC while the strain rate varies. It is

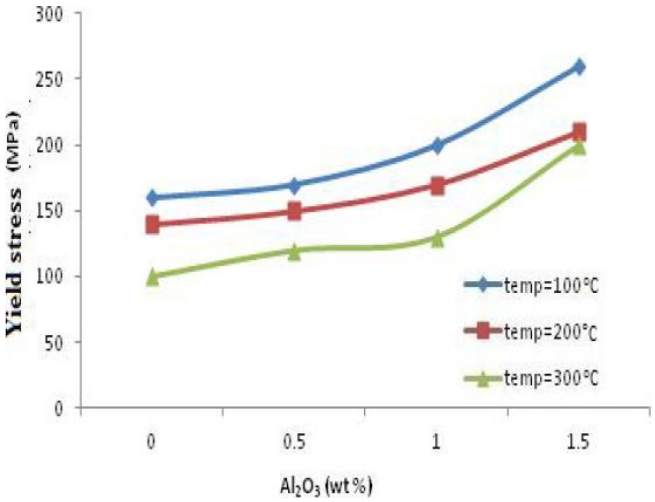

Figure 4a : The variation of yield stress as a function of ANP content at different temperatures and at a fixed strain rate of 0.01/s.

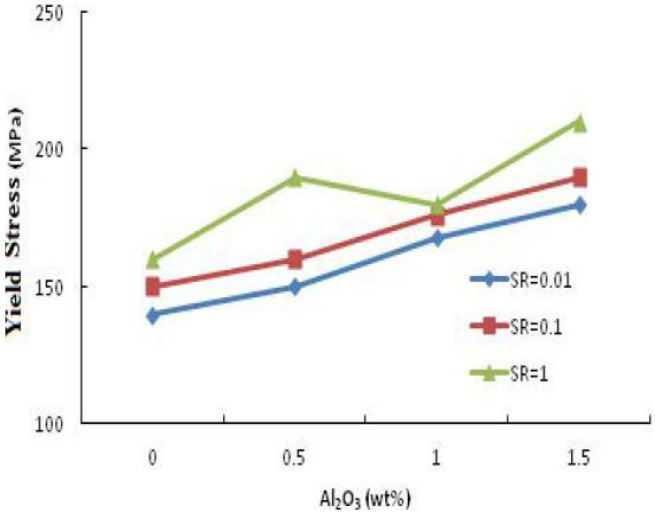

Figure 4b : The variation of yield stress with ANP content at a temperature of 200˚C and at a different strain rates

noted that, irrespective of strain rates, the yield stress increases with increase in ANP content. It is further noted that at fixed ANP content, the yield stress increases marginally with increase in strain rate. Due to increase of strain rate from 0.01 to 1/s, the yield stress increases only by 15 to 20%. If an average value, irrespective of the strain rate, is considered, the yield stress varies within ± 10%. It is again noted that the yield stress increases by 25% to 45% depending on strain rate and temperature due to addition of only 1.5 vol. % of ANP. The improvement in stress due to addition of ANP was found to be the most significant at higher temperature (300 ^oC) irrespective of strain rate (TABLE 3). This improvement of stress due to ANP addition is primarily due to

(i) coherent bonding between ANP and the matrix, and (ii) uniform distribution of ANP in the matrix this causes more restriction against grain boundary sliding and dislocation motion/ climbing. Because of the very fine particle size, inter-particle distance reduces significantly, which causes effective resistance against dislocation motion. Strong interface also facilitates greater dislocation strengthening.

The variation of ultimate compressive stress as a function of ANP content for different temperatures and at fixed strain rate of 0.01/s is shown in Figure 5a. It is evident from this figure that the ultimate stress increases steadily but slowly with increase in ANP content. Figure 5b represents variation of ultimate compressive stress with ANP content at a fixed test temperature of 200 °C while the strain rate varies. It is noted that the ultimate compressive stress increases with increase in ANP irrespective of strain rate. It is further noted that at fixed ANP content, the ultimate compressive stress increases with increase in strain rate. It is again noted that the ultimate compressive stress increases by 30% to 55% depending on strain rate and temperature due to addition of only 1.5 vol. % of ANP. The improvement in ultimate compressive stress due to addition of ANP also becomes the most effective at higher temperature (300 °C), while the improvement is of the order of 40 to 50%. This is also due to the same reason as explained earlier for increase in yield stress due to ANP addition. This is primarily because of very fine size of ANP and these are uniformly distributed in the matrix. As particles are of nano-size, these are also free from any defects. Further, particles are perfectly spherical in nature. Thus, preferential stress concentration at any point of particle surface could be avoided. Because of nano-size and perfectly spherical in nature, these particles can reorient themselves during deformation. The reorientation of these particles become much easier at higher temperature as the matrix gets soften and flows more plastically. As a result, the % elongation does not reduce significantly due to ANP addition.

It is evident from TABLE 3 that the strain hardening exponent is marginally influenced by ANP content, whereas plastic strengthening coefficient increases significantly with ANP content. It is interesting to note that in some cases; even at higher ANP content (especially at higher temperature) the strain hardening exponent is reduced. This is attributed to the fact that the dislocation generated during deformation at higher temperature generally sunk at the ANP- matrix interface. This phenomenon becomes more active due to greater possibility of dislocation climb and movement at higher test temperature. In addition, dynamic recrystallization and strain aging (causing precipitation coarsening) also leads to matrix softening. On the other hand, the deformation of the matrix gets constrained due to presence of this ANP by the way of dislocation and particle strengthening and resistance against flow of matrix materials. In general, the strength of ANPRC increases with increase in ANP content. This can be understood

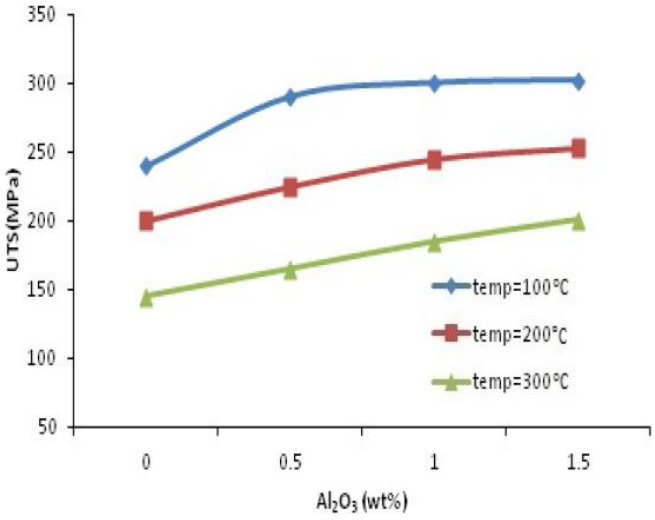

Figure 5a : The variation of ultimate compressive stress as function of ANP content for different temperature and at a fixed strain rate of 0.01/s

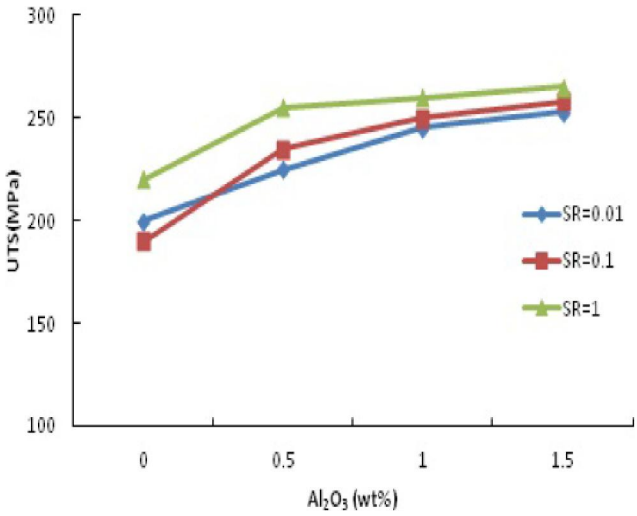

Figure 5b : The variation of ultimate compressive stress with ANP content at a temperature of 200°C and at a different strain rates

from a simple calculation. The size of ANP is in the range of 20-30 nm with an average value of 25 nm. The volume of a particle becomes 8×10^3 nm^3. Thus, per cubic micro meter of volume of ANPRC, for 0.5 vol. % ANP content, number of ANP comes to be~ 622. If it is assumed that the particles are arranged in regular array; number of particle in 1μm length falls to be ~8.5. The diameter of particle is 40 nm. Thus the inter-particle spacing comes to be ~ 90 nm. The interface spacing decreases proportionately with ANP content. At higher ANP content, the inter-particle distances reduced and the particle matrix interface area increased significantly which primarily acts as dislocation sink point. Because of very low inter-particle spacing, the matrix becomes plastically constraint to a large exponent. As a consequence of these facts, the overall strength of AANPRC increases, but the strain hardening exponent varies marginally with increase in ANP content.

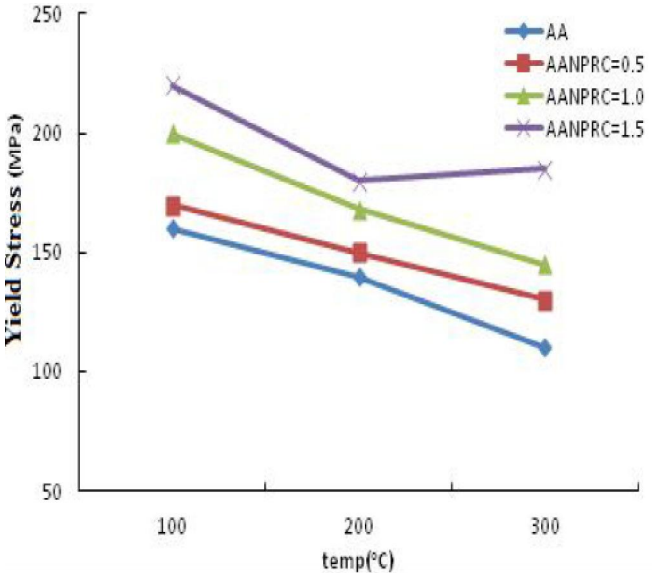

Figure 6a : The variation of yield stress as a function temperature for different ANP content and at a fixed strain rate of 0.01/s

Effect of temperature

The variation of yield stress as a function of temperature for different ANP content and at a fixed strain rate of 0.01/s is shown in Figure 6a. It is noted that the yield stress decreases with increase in temperature. It is evident that for significant improvement in the yield stress, only 1.5 vol. % ANP additions are quite effective even at higher temperatures. Similarly the variation of yield stress as a function of temperature at different strain rates for fixed ANP content of 1.0 vol. % is shown in Figure 6b. It is noted from this figure also that the yield stress decreases with temperature irrespective of the strain rate. It is further observed that the yield stress increases marginally with increase in the strain rate. The yield stress decreases monotonically with increase in temperature. The yield stress decreases by a factor of ~1/3 due to increase of temperature from 100 °C to 300 °C. The ultimate compressive stress (UCS) of ANPRC also followed the similar trend to that of yield stress with temperature under varying strain rates (Figure 7a) and ANP content (Figure 7b). These figures demonstrate that the UCS decreases with increase in temperature irrespective of ANP content and strain rate. The extent of reduction is around 1/3 to ½ due to increase of temperature from 100 °C to 300°C. The elongation on the other hand increases significantly with temperature. At 300°C the material did not fractured or cracked. The cylindrical sample reshaped into a coin without showing any crack irrespective of strain rate and ANP content. It is worth noting that AANPRC (up to 1.5 vol. % ANP) deformed effectively (more than 100%) at a temperature of 300 °C. This indicates that at high temperature, even 1.5 vol. % ANP reinforced AANPRC deformed super-plastically at a temperature >200°C. It is to be noted that the strength of AANPRC increased significantly and deformed super plastically also, signifying that these AANPRC can be rolled or

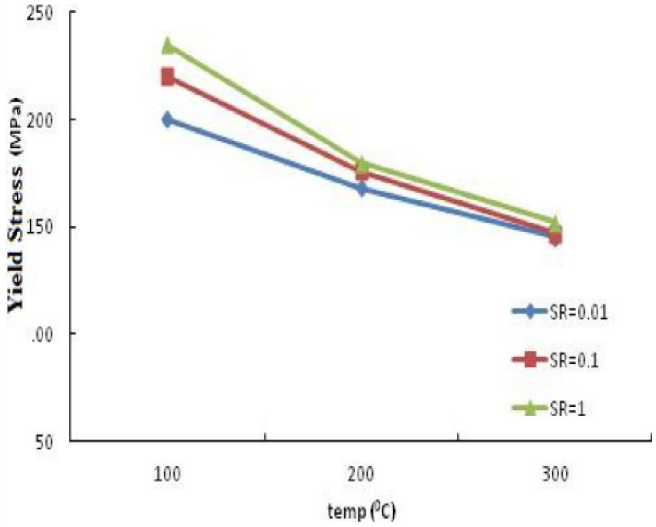

Figure 6b : The variation of yield stress as a function of temperature at different strain rates for fixed ANP content of 1.0 vol %

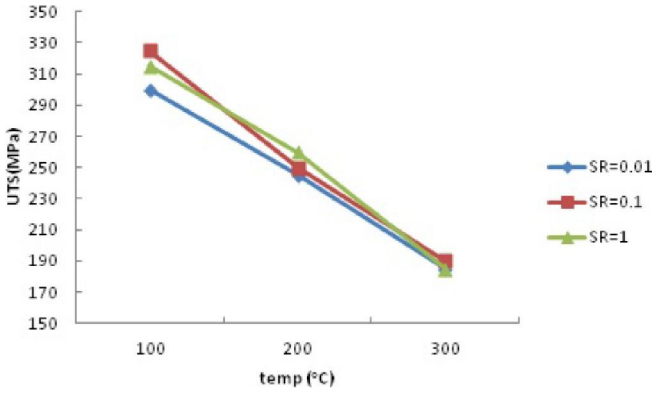

Figure 7a : The variation of ultimate compressive stress of AANPRC with temperature under varying strain rates

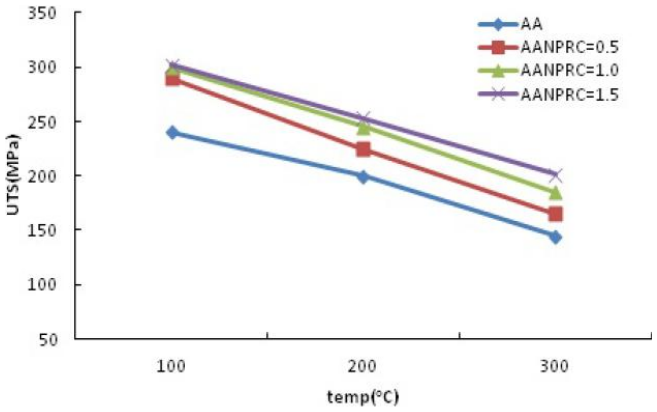

Figure 7b : The variation of ultimate compressive stress of AANPRC with temperature under varying ANP contents

extruded effectively for making sheets, plates and tubes for structural application.

Effect of strain rate

The variation of *ln* (σ_Y) as a function of *ln* (*έ*) for varying ANP content is shown in Figure 8a. Similarly the variation of *ln* (σ_Y) with of *ln* (*έ*) for different temperature at fixed ANP content of 1.0 vol. % is shown in Figure 8b. It is evident from these figures that the yield stress increases marginally with strain rate. In few cases, the variation of yield stress is very nominal. This trend is noted irrespective of temperature and ANP content. In order to calculate the strain rate sensitivity, the slope of the best fitted linear plots of *ln* (σ_Y) vs. *ln* (*έ*) are recorded and reported in TABLE 4. Similarly, the variation of ln (UCS) with ln (έ) for different temperature at fixed ANP content is shown in Figure 9. It is evident from this figure, that like the yield stress, the UCS also either increased marginally or remained almost invariant with strain rate. The values of slope in best linearly fitted *ln* (σ_{UCS}) vs *ln* (*έ*) are also calculated and reported

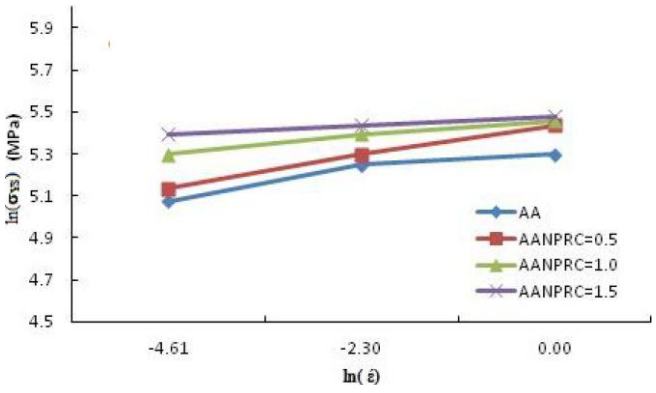

Figure 8a : The variation of ln (σ_{YS}) as a function of ln (έ) for varying ANP contents

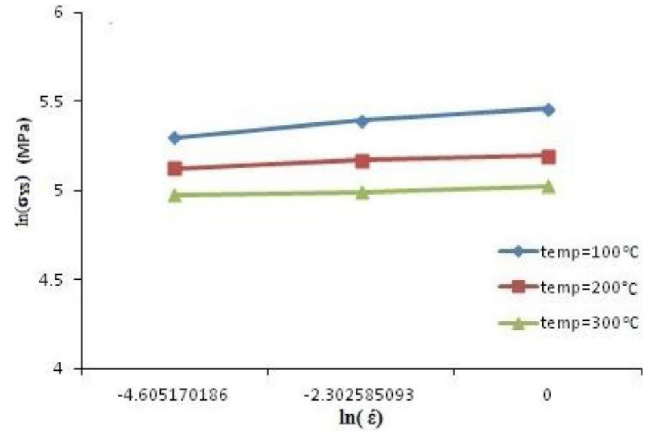

Figure 8b : The variation of ln (σ_{YS}) as a function of ln (έ) for different temperature at fixed ANP content of 1.0 vol%. ln (σ_{YS})

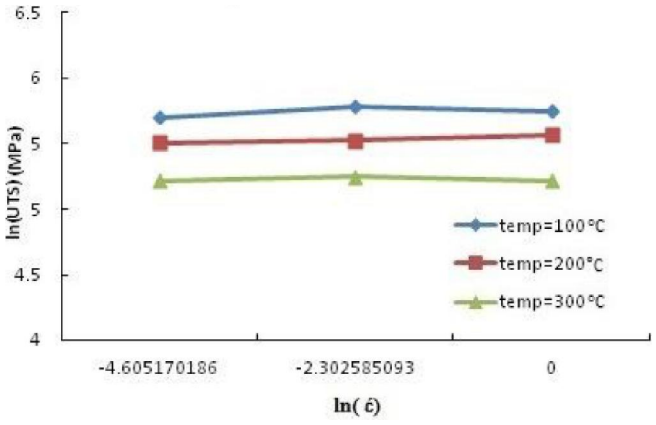

Figure 9 : The variation of ln (UCS) as a function of ln (έ) for different temperature at fixed ANP content of 1.0 vol%

in TABLE 4. The slope for the plot of yield stress and UCS are reported as m_{Ys} and m_{UCS} respectively. Similarly, the strain rate strengthening coefficient 'K_S' from the antilog of intercept of *ln* (σ_y) vs. *ln* (*έ*) best fitted linear plot is referred as K_{Ys} and that of *ln* (σ_{UCS}) vs. *ln* (*έ*) best fitted linear plot is referred as K_{UCS}. The values

Full Paper

TABLE 4 : Effect of % ANP content and temperature on strain rate sensitivity ('m_{YS}' or 'm_{UCS}') and strengthening co-efficient (K_{YS} or K_{UCS})

	Al_2O_3 (vol %)	Temp (^{0}C)	m_{ys}/m_{ucs}	$K_{ys}/_{Kucs}$ (MPa)
ln Ys Vs ln (SR)	0.0	100	0.111	145.91
		200	0.066	130.97
		300	0.055	105.10
	0.5	100	0.151	146.64
		200	0.118	130.84
		300	0.037	123.71
	1.0	100	0.08	185.30
		200	0.034	162.87
		300	0.023	141.03
	1.5	100	0.043	210.60
		200	0.077	165.33
		300	-0.072	189.99
ln UTS Vs ln (SR)	0.0	100	0.077	223.63
		200	0.047	184.38
		300	0.049	138.79
	0.50	100	0.013	288.01
		200	0.062	209.97
		300	0.009	164.51
	1.0	100	0.024	297.97
		200	0.029	236.98
		300	0	186.60
	1.5	100	0.036	291.48
		200	0.023	246.90
		300	0.021	196.36

of m_{ys} or m_{UCS} and K_{ys} or K_{UCS} are reported in TABLE 4. It is evident from this table that both $m_{\sigma y}$ and m_{UCS} are very low irrespective of ANP content. However, amongst the investigated materials, $m_{\sigma y}$ and m_{UCS} are noted to be marginally higher for AA. As a whole, these values are almost invariant to the type of material. But, the value of K_{ys} or K_{UCS} decreases significantly with increase in temperature and increases considerably with ANP content. These results thus suggest that the compressive deformation response of these materials (alloys and composites) is almost invariant to the strain rate irrespective of temperature and ANP content. However, the deformation response of these alloys and composites is significantly influenced by the temperature and ANP content. As at higher temperature K_{ys} or K_{UCS} is reduced significantly. All these investigated materials deformed quite effectively at elevated temperature.

Microstructure evolution after deformation

The microstructure of AANPRC after deformation at 200^{o}C and at a strain rate of 0.01/s is shown in Figure 10a. It is clear that α-aluminium grains deformed significantly, which in due course led to a lamellar grain structure. The eutectic phase and $CuAl_2$ intermetallic flow along the grain boundary and finally led to fine micro- cracks (arrow marked) and micro voids (marked 'V'). During deformation ANPs also flow with the matrix (marked 'N'). At higher magnification, matrix shows large number of submicron precipitates and ANPs distributed uniformly in the matrix as shown in Figure 10b. The coarser eutectic phase or the intermetallic phase get fragmented and distributed along the grain boundary. The precipitates and ANPs seem to be rearranged them along the sub-grain boundaries (arrow marked) generated due to dynamic recrystallization (Figure 10c). Greater extent of recrystallization and strain aging were

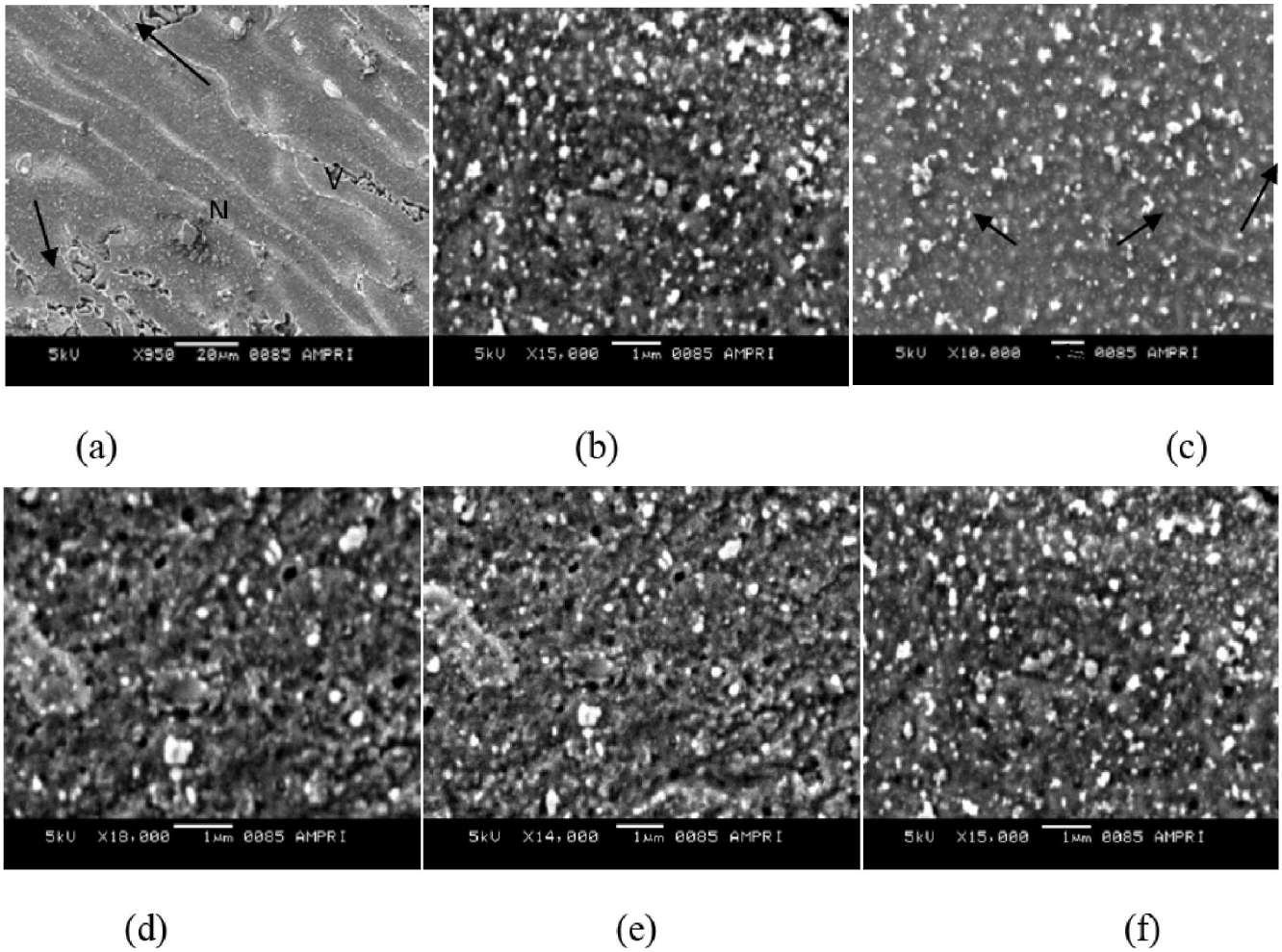

Figure 10 : Microstructure of AANPRC after deformation (a) at 200^{O}C and ε = 0.01/s, (b) submicron and ANP, in matrix, (c) particles and precipitates along grain boundary, (d) recrystallised and strain aging at 300^{0}C, (d) AANPRC with 1 vol% ANP, (e) AANPRC with 1.5 vol%, ANP having higher amount of precipitation, (f) AANPRC with 1.5 vol%, ANP at strain rate of 1.0/ s and at temperature of 300^{O}C.

TABLE 5 : Nano-hardness and Young's modulus with respect to ANP contents before and after deformation

S.N.	Al_2O_3 content (vol%)	Before deformation		Deformation Temp (^{O}C)	Strain Rate (S^{-1})	Strain	After deformation	
		Nano-hardness (Kg/mm^2)	Young's Modulus (GPa)				Nano-hardness (Kg/mm^2)	Young's Modulus (GPa)
1	0.0	71.3	65.5					
				100	0.01		74.3	63.5
2	0.5	85.0	89.0	RT				
				100	0.01		78.9	82.5
				200	0.01		30.5	35.5
					0.1		48.3	38.01
					1.0		52.1	38.19
3	1.0	92.3	95.8	200	0.01	0.05	45.6	49.2
						0.10	43.3	44.5
						0.15	38.3	40.5
						0.20	34.3	37.2
4	1.5	102.5	112.5					

observed when the samples were deformed at higher temperature (300°C) (Figure 10d). This demonstrates the fact that at higher temperature, the dynamic recrystallization and strain aging are more prevalent. These lead to more softening of the matrix and thus the matrix flow more easily during plastic deformation. Very fine nano-particles also flow along with the matrix. When ANP content increased to 1.5 vol. %, the extent of precipitation and recrystallization is relatively higher which can be understood from the presence of more precipitation and finer sub-grain sizes (Figure 10e). This is primarily due to higher strain energy in the matrix due higher ANP content. As a result, it is expected that aging kinetics would also be faster and there would be the possibility of precipitation coarsening due to dynamic strain aging leading to matrix softening. However, the distance between ANP particles reduced significantly when the ANP particle increased to 1.0 or 1.5 vol%. This makes the matrix plastically constraint as a whole. Thus, the AANPRC retains their strength even at high temperature, though locally the matrix gets softened. When the same AANPRC is tested at same temperature but at higher strain rate (1.0/s), the matrix microstructure Figure 10f is noted to be almost similar to that observed in Figure 10e. The matrix softening due to precipitation coarsening and dynamic recrystallization is also reflected in the nano-hardness measurement (TABLE 5). Both the nano-hardness and the modulus are reduced when AANPRC was deformed at high temperature. This is attributed to dynamic strain aging and recrystallization.

CONCLUSIONS

The following conclusions can be drawn from the present studies:

ANP particles can be successfully distributed uniformly through addition of small pallets of ANP and aluminum powder mixture (ANP: Al=3:7) simply by mechanical stirring. Thus, AANPRC with uniform ANP distribution can be made.

Only 1.5 vol% of ANPs is sufficient to improve the hardness and strength of AANPRC by ~20%.

The extent of ANP segregation increases at higher ANP content. The bonding between nano-particles and matrix is quite coherent and strong.

At lower temperature strain hardening is noted during deformation. But at higher temperature, strain softening is observed. This may be due to dynamic recrystallization and dynamic strain aging of the matrix. Strain hardening exponent and plastic strengthening increase with increasing ANP content, and decrease with temperature.

The strength and other deformation parameters are strongly influenced by ANP content and temperature, but almost constant or marginally varied with strain rate. The strain rate sensitivity parameter is measured to be very low (<0.1). But the strain rate strengthening coefficient increased significantly with ANP content.

During deformation strain aging is also observed. Dynamic recrystallization and strain aging of matrix control the deformation behavior of nano Al_2O_3 particle reinforced composite especially at higher temperature.

ACKNOWLEDGEMENTS

Authors are thankful to Director, CSIR-AMPRI for funding to conduct this work and also giving his approval to publish this work.

REFERENCES

[1] Ali Mazahery, Mohsen Ostadshabani; Investigation on mechanical properties of nano-Al2O3- reinforced aluminium matrix composites, Journal of Composite Materials, **45(24)**, 2579-2586 **(2011)**.

[2] T.G.Durai, Karabi Das, Siddhartha Das; Synthesis and characterization of Al matrix Composites reinforced by in situ alumina particulates, Material Science and Engineering A, **445-446**, 100-110 **(2007)**.

[3] Hai Su, Wenli Gao, Zhaohui Feng, Zheng Lu; Processing microstructure and tensile properties of nano-sized Al2O3 particle reinforced aluminium matrix composites, Materials and Design, **36**, 590-596 **(2012)**.

[4] S.M.Suresh, Debadutta Mishra, A.Srinivasan, R.M.Arunachalam, R.Sasikumar; Production and characterization of micro and nano Al2O3 particle-reinforced LM25 aluminium alloy composites, ARPN Journal of Engineering and Applied Sciences, **6**, 94-98 **(2011)**.

[5] Guirong Li, Honngming Wang, Xueting Yuan, Yutao Zhao; Microstructure of nanometer Al2O3 particles reinforced aluminium matrix composites processed by high pulsed field, Materials Letters, **99**, 50-53 **(2013)**.

[6] A.Ansary Yara, M.Montazerianb, H.Abdizad, H.R.Baharvandic, Microstructure and Mechanical Properties of Aluminium Alloy Matrix Composite Reinforced with Nano-particle MgO, Journal of Alloys and compounds, **484**, 400-404 **(2009)**.

[7] J.Hashim, L.Looney, M.S.J.Hashmi; Metal Matrix Composites production by the stir casting method, Journal of Material Processing Technology, **92-93**, 1-7 **(1999)**.

[8] Pay Yih, Deborah D.L.Chung; Powder Metallurgy Fabrication of Metal matrix Composite Using Coated Filler, The International Journal of Powder metallurgy, **31**, 335-340 **(1995)**.

[9] Yong Yang, Jie Lan, Xiaochun Li; Study on bulk aluminium matrix nano-composite fabricated by ultrasonic dispersion of nano-sized SiC particles in molten aluminium alloy, Materials Science and Engineering: A, **380**, 378-383 **(2004)**.

[10] B.Ramesh, T.Senthilvelan; Formability Characteristics of Aluminium based composites- A Review, IACSIT International Journal of Engineering & Technology, **2**, 1-6 **(2010)**.

[11] Nikhilesh Chawla, Yu-Lin Shen; Mechanical Behaviour of Particle reinforced metal Matrix Composite, Advanced Engineering Materials, **3**, 357-369 **(2001)**.

[12] Rupa Dasgupta, A.KJha, S.Das; Effect of addition of SiC Particles on the Dry sliding Wear behaviour extruded 2014 Al- Alloy, ISRN Tribology, **2013**, 1-9 **(2013)**.

[13] M.S.Song, M.X.Zhang, S.G.Zhang, B.Huang, J.G.Li; In Situ Fabrication of TiC particulates locally reinforced aluminium matrix composites by self-propagating reaction during casting, Materials Science, **473**, 166-171 **(2008)**.

[14] E.Darmiani, I.Danaee, M.A.Golozar, M.R.Toroghinejad, A.Ashrafi, A.Ahmadi; Reciprocating wear resistance of Al-SiC nano-composite fabricated by accumulative roll bonding process, Materials and Design, **50**, 497-502 **(2013)**.

[15] Manoj Singla, D.Deepak Dwivedi, Lakhvir Singh, Vikas Chawla; Development of Aluminium Based Carbide Particulate Metal Matrix Composite, Journal of Minerals &Materials Characterization & Engineering, **8**, 455-467 **(2009)**.

[16] C.Y.Liu, Q.Wang, Y.Z.Jia, B.Zhang, R.Jing, M.Z.Ma, Q.Jing, R.P.Liu; Evaluation of mechanical properties of 1060-Al reinforced with WC particles via warm accumulative roll bonding process, Materials and Design, **43**, 367-372 **(2013)**.

[17] S.B.Venkata Siva, R.I.Ganguly, G.Srinivasarao, K.L.Sahoo; Machinability of Aluminium metal matrix composite reinforced with In –situ ceramic composite developed from mines waste colliery Shale, Materials and Manufacturing Processes, **28**, 1082-1089 **(2013)**.

[18] H.Boutefnoucheta, C.Curfsb, A.Trikia, A.Boutefnouchetc, D.Vrel; Self-Propagating high-temperatu re Synthesis mechanism within the Ti-C-Ni system: A time resolved X-ray diffraction study, Powder Technology, **217**, 443-450 **(2012)**.

[19] Metal Hand Book Metallographic & Microstructure (Edited by George F. Vender Voort), Published by ASM international, OH, USA, **9 (2004)**.